

A transferable *ab-initio* based force field for aqueous ions

Sami Tazi, John J. Molina, Benjamin Rotenberg, Pierre Turq, and Mathieu Salanne

*UPMC Univ Paris 06, CNRS, ESPCI,
UMR 7195 PECSA, F-75005 Paris, France*

Rodolphe Vuilleumier

*UPMC Univ Paris 06, Ecole Normale Supérieure,
Département de Chimie, F-75231 Paris, France*

Abstract

We present a new polarizable force field for aqueous ions (Li^+ , Na^+ , K^+ , Rb^+ , Cs^+ , Mg^{2+} , Ca^{2+} , Sr^{2+} and Cl^-) derived from condensed phase *ab-initio* calculations. We use Maximally Localized Wannier Functions together with a generalized force and dipole-matching procedure to determine the whole set of parameters. Experimental data is then used only for validation purposes and a good agreement is obtained for structural, dynamic and thermodynamic properties. The same procedure applied to crystalline phases allows to parametrize the interaction between cations and the chloride anion. Finally, we illustrate the good transferability of the force field to other thermodynamic conditions by investigating concentrated solutions.

I. INTRODUCTION

The development of classical force fields for ions in aqueous solution is essential to the description of specific effects, which are legion in biochemistry¹⁻³, atmospheric chemistry⁴ or environmental science⁵. The reliability of molecular simulations strongly depends on the quality of the force field used to represent the interactions, which must capture not only the effects of ionic size, but also the polarization of water by the ionic charge. The latter multi-body effect becomes essential when dealing with multivalent ions⁶, in concentrated solutions⁷ and in interfacial environments^{4,8,9}.

In recent years, a successful strategy to derive polarizable force fields for solid and molten oxides from *ab-initio* simulations has been developed by Madden and co-workers¹⁰⁻¹². A full set of parameters was obtained for the Ca-Mg-Al-Si-O (CMAS) system¹³, which is the main component of the Earth's crust and mantle. Cation-rich aluminosilicates, including clays and zeolites, are also the principal minerals on the Earth's surface, where they are in contact with ionic solutions. Examples of situations where the interface between such minerals and solution play an important role include the crystallization and dissolution of ionic crystals, such as calcium carbonate (in the context of carbon dioxide sequestration¹⁴) or sodium sulfate (deterioration of monuments¹⁵), or the sorption of radioactive contaminants (e.g. cesium or strontium) onto clays^{16,17}. It is therefore of primary importance to extend the CMAS force field in order to describe these minerals and their interaction with water and ions. As a first step in this direction, we develop here a polarizable force field for ions in water which is compatible with that developed for the CMAS system.

As mentioned previously, and despite the success of non-polarizable water force fields in the bulk¹⁸⁻²¹, transferability to interfaces, especially charged ones, requires resorting to a polarizable model. Many such models exist, which differ mainly in their treatment of the polarizability. Drude or shell models assign a charge on a spring to each polarizable atom²²⁻²⁴. Other approaches allow for charge fluctuations^{25,26} or assign point dipoles to each polarizable species²⁷⁻³¹. Only the latter model is compatible with the above-mentioned one for oxides. Among the point polarizability models, we chose the one of Dang and Chang which was specifically developed to describe the gas-liquid interface²⁹. In addition, Masia *et al.* have shown that it accurately reproduces the strong water polarization by divalent cations^{32,33}.

Following the strategy of Madden and co-workers, which has proven able to simultaneously reproduce structural, dynamic and thermodynamic properties not only for the CMAS system, but also for many other ionic materials^{11,12,34,35}, we derive here the parameters of a force field for the aqueous ions: (Li⁺, Na⁺, K⁺, Rb⁺, Cs⁺, Mg²⁺, Ca²⁺, Sr²⁺ and Cl⁻). The route from condensed phase Density Functional Theory (DFT) calculations, using Maximally Localized Wannier Functions (MLWFs)^{36,37} together with a generalized force and dipole-matching procedure^{38,39}, renders experimental input unnecessary, contrary to many force field parametrizations.

The paper is organized as follows: We first give a detailed description of the force field and its parametrization which involves DFT calculations on single ions in bulk water and on ionic crystals. The second part is then devoted to the validation of the model, against structural, dynamic and thermodynamic properties of these systems. Finally, the transferability of the model is illustrated by the study of concentrated salt solutions.

II. THE FORCE FIELD AND ITS PARAMETRIZATION

A. Model

The total energy of the system is decomposed into four terms:

$$V_{\text{tot}} = V_{\text{charge}} + V_{\text{disp}} + V_{\text{rep}} + V_{\text{pol}} \quad (1)$$

For the calculation of the direct Coulomb interaction between two atoms I and J ,

$$V_{\text{charge}} = \sum_{I,J>I} \frac{q^I q^J}{r_{IJ}} \quad (2)$$

formal charges (here -1 , $+1$ or $+2$) are used. The dispersion potential includes the dipole-dipole and dipole-quadrupole terms

$$V_{\text{disp}} = - \sum_{I,J>I} \left[f_6^{IJ}(r_{IJ}) \frac{C_6^{IJ}}{r_{IJ}^6} + f_8^{IJ}(r_{IJ}) \frac{C_8^{IJ}}{r_{IJ}^8} \right] \quad (3)$$

and the short-range corrections are described using the Tang-Toennies functions f_n^{IJ} , which are of the form⁴⁰:

$$f_n^{IJ} = 1 - e^{-b_D^{IJ} r_{IJ}} \sum_{k=0}^n \frac{(b_D^{IJ} r_{IJ})^k}{k!} \quad (4)$$

While the repulsion potential is modelled using a decaying exponential:

$$V_{\text{rep}} = \sum_{I,J>I} A^{IJ} e^{-B^{IJ} r_{IJ}} \quad (5)$$

Finally, many-body electrostatic effects are described by the induced dipoles μ^I , which are treated as additional degrees of freedom and obtained at each MD step by minimizing the polarization energy:

$$V_{\text{pol}} = \sum_I \frac{1}{2\alpha^I} |\mu^I|^2 + \sum_{I,J} \left[(q^I \mu_\alpha^J g^{IJ}(r_{IJ}) - q^J \mu_\alpha^I g^{JI}(r_{IJ})) T_{IJ}^\alpha - \mu_\alpha^I \mu_\beta^J T_{IJ}^{\alpha\beta} \right] \quad (6)$$

with α^I the ion polarizability and where the Einstein summation convention is assumed. A short-range correction to the multipolar expansion of the Tang-Toennies type is used:

$$g^{IJ}(r_{IJ}) = 1 - c^{IJ} e^{-b^{IJ} r_{IJ}} \sum_{k=0}^4 \frac{(b^{IJ} r_{IJ})^k}{k!} \quad (7)$$

This so-called Polarizable Ion Model (PIM) has proven extremely successful for the description of oxides, chloride and fluoride-based materials, both in the solid and liquid states^{11,12,34}. Water is described by a model compatible with this form, developed by Dang and Chang²⁹. The only differences with the PIM are the description of the repulsive and dispersion terms $V_{\text{rep}} + V_{\text{disp}}$ for the water-water interactions, represented by a Lennard-Jones potential, and the absence of short-range damping of the charge-dipole interaction. The Dang-Chang (DC) water is a rigid 4-site model, with an additional virtual site M along the symmetry axis of the molecule, which bears a negative partial charge, as well as the induced dipole, while the Lennard-Jones interaction acts on the oxygen atom only. The parameters of the DC model are summarized in Table I.

d_{OH} Å	d_{OM} Å	angle (°)	ϵ_{O} (kcal/mol)	σ_{O} Å	q_{H}	α_{M} Å
0.9752	0.215	104.52	0.1825	3.2340	0.5190	1.444

TABLE I: Parameters of the Dang-Chang water model.

The purpose of the present work is to derive all the parameters of the PIM for water-ion and ion-ion interactions, thereby providing a force field for the simulation of ions which is transferable from infinite dilution to concentrated solutions, up to the ionic crystals, for alkaline (Li^+ , Na^+ , K^+ , Rb^+ , Cs^+) and alkaline earth (Mg^{2+} , Ca^{2+} , Sr^{2+}) cations and the

chloride (Cl^-) anion. Overall, this requires specifying 241 parameters. The procedure to determine all of them from *ab-initio* calculations aims at minimizing the risk of compensation of errors among the different terms by 1) directly computing as many parameters as possible, 2) adjusting the remaining ones on different quantities (dipoles and forces) and 3) resorting to simplifying assumptions when necessary. We now describe these three aspects.

B. Calculating parameters

First-principle calculations based on Density Functional Theory (DFT) describe the electronic density using the Kohn-Sham orbitals, whose delocalized nature renders the assignment of atomic or molecular properties difficult. The concept of the maximally localized Wannier function (MLWF) provides a convenient framework to analyze atomic and molecular properties in the condensed phase⁴¹. The Wannier functions are defined through a unitary transformation of the Kohn-Sham eigenvectors. MLWFs are constructed by choosing the phase so that it minimizes the spread of the Wannier function⁴¹. It was shown recently that MLWFs could be used to systematically derive both the polarizabilities α^I and dispersion parameters C_6^{IJ} and C_8^{IJ} of a PIM^{37,39}. Figure 1 illustrates the electronic density around a Ca^{2+} cation and two water molecules in bulk water, reconstructed from their respective Wannier orbitals.

1. Polarizability

In a closed shell system, each MLWF contributes two electrons, so that the atomic or molecular dipole can be computed (in atomic units) as

$$\boldsymbol{\mu}^I = \sum_{i \in I} (Z_i \mathbf{R}_i - 2 \sum_{n \in i} \mathbf{r}_n^w) \quad (8)$$

where the sums run over atoms i belonging to fragment I and over MLWFs $n \in i$ whose center is localized in the vicinity of the nuclear position \mathbf{R}_i , Z_i is the charge of nucleus i and \mathbf{r}_n^w is the position of the center of the n -th MLWF. The polarizability may differ from that of the same ion in the gas phase because of environmental effects. It can be calculated by applying a small electric field $\boldsymbol{\mathcal{E}}^{(\alpha)}$ along each Cartesian direction $\alpha = x, y, z$ to the system, which induces dipole moments $\{\delta \boldsymbol{\mu}^{I,(\alpha)}\}_{I \in [1, N]}$. A convenient way to distinguish the effect of

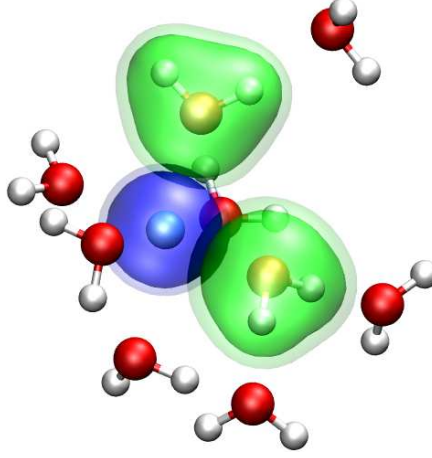


FIG. 1: Localized electronic density around a Ca^{2+} cation and two water molecules in bulk water, reconstructed from their respective Wannier orbitals. The isodensity surfaces include 90 % and 95 % of the corresponding densities, respectively.

the applied field from that of the static fields caused by the permanent charge distributions of the molecules, is to think of the former as an optical field. $\delta\mu^I$ can then be seen as the net induced dipole oscillating at the optical frequency. The total field $\mathbf{f}^{I,(\alpha)}$ on each atom is

$$\mathbf{f}^{I,(\alpha)} = \boldsymbol{\mathcal{E}}^{(\alpha)} + \sum_{J \neq I} \mathbf{T}^{IJ} \cdot \delta\boldsymbol{\mu}^J(\mathbf{R}^N) \quad (9)$$

where \mathbf{T}^{IJ} is the dipole-dipole interaction tensor. The polarizability tensor of molecule I can then be obtained by inverting Eq. (9) :

$$\boldsymbol{\alpha}^I(\mathbf{R}^N) = (\mathbf{F}^I)^{-1} \cdot \boldsymbol{\Pi}^I \quad (10)$$

with the second-rank three dimensional tensors defined as : $F_{\alpha\beta}^I = f_{\alpha}^{I,(\beta)}$ and $\Pi_{\alpha\beta}^I = \delta\mu_{\alpha}^{I,(\beta)}$. More details about this approach can be found in Ref.⁴².

2. Dispersion: C_6 and C_8

DFT calculations do not usually account for dispersion interactions, because the former describe the electronic ground state while the latter arise from correlated density fluctuations associated with excited states. The treatment of dispersion via non-local functionals has only recently been introduced, albeit at a high computational cost. Thus these interactions are generally added (if at all) as an *a posteriori* correction. Among the several methods that have been proposed for computing this correction, the method of Grimme⁴³ and that of Silvestrelli⁴⁴ seem to be the most popular. In this work we use the latter, which considers the dispersion interaction between all pairs of MLWF as follows. The long-range interaction between separated fragments of matter is calculated, following Andersson et al.⁴⁵, as

$$E_{xc}^{lr} = \frac{6e}{4(4\pi)^{3/2}m^{1/2}} \iint_{V_1 V_2} d\mathbf{r}_1 d\mathbf{r}_2 \frac{\sqrt{\rho_1(\mathbf{r}_1)\rho_2(\mathbf{r}_2)}}{\sqrt{\rho_1(\mathbf{r}_1)} + \sqrt{\rho_2(\mathbf{r}_2)}} \times \frac{1}{\|\mathbf{r}_1 - \mathbf{r}_2\|^6} \quad (11)$$

where $\rho(r_i)$ is the charge density of fragment i , m the electron mass and V_i the volume occupied by fragment i . For large separations R , this scales as $E^{lr} = -C_6/R^6$, where the C_6 coefficient for the interaction between two MLFWs k and l can be computed as :

$$C_6^{kl} = \frac{3}{32\pi^{3/2}} \iint_{\substack{r_1 \leq r_c \\ r_2 \leq r'_c}} d\mathbf{r}_1 d\mathbf{r}_2 \frac{w_k(\mathbf{r}_1)w_l(\mathbf{r}_2)}{w_k(\mathbf{r}_1) + w_l(\mathbf{r}_2)} \quad (12)$$

The cut-off radius $r_c = (1.475 - 0.866 \ln S)S$ is chosen to correctly capture the limit of long-range perturbations in an electron gas⁴⁴. The MLWFs, giving rise to densities $\rho = w^2$, are assumed to be of the Slater form:

$$w_n(\|\mathbf{r} - \mathbf{r}_n\|) = \frac{3^{3/4}}{\sqrt{\pi}S_n^{3/2}} e^{-(\sqrt{3}/S_n)\|\mathbf{r} - \mathbf{r}_n\|} \quad (13)$$

characterized solely by their spread $S_n = \langle w_n | r^2 | w_n \rangle - \langle w_n | r | w_n \rangle^2$ and center r_n .

We have previously shown that the dispersion interaction between two ensembles of charge density fragments can be obtained from the averaged sum over pair interactions of MLWFs³⁷. Assuming an isotropic distribution of MLWF centers around the nuclei I and J , at fixed distances, leads (to second leading-order) to $V_{disp} = -\sum_{n=6,8} C_n^{IJ}/r_{IJ}^n$, where the dispersion

coefficients are:

$$C_6^{IJ} = \sum_{k \in I, l \in J} C_6^{kl} \quad (14)$$

$$C_8^{IJ} = \sum_{k \in I, l \in J} 5(d_k^2 + d_l^2) C_6^{kl} \quad (15)$$

where $d_{k,l}$ are the distances of the MLWF centers to their respective nuclei and C_6^{kl} is computed for each pair of MLWFs according to Eq. 12. The determination of the parameter b_D in Eq. 4, for the short-range damping of the dispersion interaction, is detailed below.

C. Dipole- and force-fitting

Not all parameters of the force field can be derived systematically from the electronic density. However, they can be determined numerically so as to best reproduce the atomic properties calculated by DFT: the total dipoles (permanent plus induced) of ions and molecules and the forces acting on them.

1. Damping of charge-dipole interaction

The first step in our parametrization procedure is to determine the parameters involved in Eq. 7 for the short-range damping of the charge-dipole interaction. This is achieved by numerically adjusting these parameters so as to minimize the error on the dipoles calculated using the classical force field, relative to the DFT ones on a number of representative configurations:

$$\chi_\mu^2 = \frac{1}{N_{\text{conf}}} \frac{1}{N_{\text{atom}}} \sum_{\text{conf}} \sum_{\text{atom}} \frac{||\boldsymbol{\mu}^{\text{classical}} - \boldsymbol{\mu}^{\text{DFT}}||^2}{||\boldsymbol{\mu}^{\text{DFT}}||^2} \quad (16)$$

Together with the polarizabilities, these parameters complete the description of the polarization potential V_{pol} .

2. Repulsion

The parameters of the repulsive potential V_{rep} in Eq. 5 can then be obtained by a similar procedure as the one used for the dipoles, if the functional used for the DFT calculation

does not include dispersion interactions (e.g. PBE or BLYP)^{46,47}:

$$\chi_F^2 = \frac{1}{N_{\text{conf}}} \frac{1}{N_{\text{atom}}} \sum_{\text{conf}} \sum_{\text{atom}} \frac{\|\mathbf{F}^{\text{classical}} - \mathbf{F}^{\text{DFT}}\|^2}{\|\mathbf{F}^{\text{DFT}}\|^2} \quad (17)$$

By adjusting the parameters for the damping of the charge-dipole interaction and for the repulsion on different physical quantities (dipoles and forces, respectively), we limit the risk of having a compensation of errors between the different terms of the potential.

D. Further considerations

The water-ion interactions are parametrized by applying the procedure described above on configurations of a system containing a single ion in bulk water. For the ion-ion interactions, we use configurations of the experimentally stable crystal phase under normal conditions: NaCl structure for Li^+ , Na^+ , K^+ and Rb^+ , CsCl structure for Cs^+ , MgCl_2 structure for Mg^{2+} , and CaCl_2 structure for Ca^{2+} and Sr^{2+} . The Cl-Cl interactions must be the same among the different crystals in order to ensure the consistency and transferability of our potentials. The parameters for the Cl-Cl repulsion are obtained for LiCl, in which they are the most prominent, and the corresponding values are then used for all crystals. The C_6 and C_8 parameters for the Cl-Cl dispersion interaction are obtained by averaging the values for the different crystals.

For the cation-anion repulsion (see Eq. 5), the force-fitting procedure results in B parameters that are very close to each other among the alkaline ions on the one hand, and among the alkaline earth ions on the other hand. For the sake of simplicity, we use only one value for this parameter for each ion series. The A parameters for the cation-anion repulsion are then readjusted to minimize Eq. 17 while keeping the B value fixed. The final values for A and the corresponding χ_F^2 were practically unchanged by this constraint, thus confirming the relevance of this choice.

In order to further decrease the number of free parameter, the range of the short-range damping used for the cation-anion dispersion b_D^{IJ} (see Eqs. 3 and 4) is taken in most cases equal to that of the short-range repulsion B^{IJ} . This assumption is not new⁴⁸, and it is justified by the notion that the long-range scaling of dispersion breaks down as the electronic fragments start overlapping, when the short-range repulsion comes into play. The damping of the Cl-Cl dispersion is adjusted numerically so as to reproduce simultaneously the

experimental density of all crystals. For the largest cations, Cs^+ and Sr^{2+} , a value slightly smaller than $B^{\text{cation-Cl}}$ was needed to reproduce the experimental densities. Compared to the usual procedure of parametrizing a PIM from *ab-initio* simulations^{11,34}, the systematic determination of the C_6 and C_8 coefficients and the assumption that $b_D = B$ dramatically reduce the number of parameters that need to be adjusted in order to reproduce the whole set of experimental densities. The damping parameter of the monovalent cation-water dispersion interaction was chosen equal to that for the corresponding monovalent cation- Cl^- dispersion interaction $b_D^{\text{ion-O}} = b_D^{\text{ion-Cl}}$, since the water molecules and the Cl^- ions have approximately the same size. As far as the divalent cations are concerned, the attractive force arising at short distances from dispersion is negligible compared to the charge-charge and charge-dipole interactions. We can thus omit damping this interaction without any loss of accuracy. Similarly, the dispersion interaction between Cl^- and water oxygen atom is not damped.

Overall, these considerations reduce the number of parameters for the interaction of all ions with water and of cations with chloride from 241 to 187, after the neglect of some terms for the reasons explained above, and to 170 by further assuming that the ranges of some interactions are equal. Out these 170, only 82 are adjusted numerically from the dipole- and force-matching procedures of section II C, while the rest are computed as explained in section II B.

E. Simulation details

The parametrization of the force field from *ab-initio* simulations is achieved using representative configurations of the aqueous ions and the ionic crystals. For each ionic species, ~ 100 configurations of a system containing a single ion and 32 water molecules are generated using the force-field of Dang *et al.*^{49–51} for the monovalent ions, and that of Yu *et al.*⁵² for the divalent ions. DFT calculations were then performed on these configurations with the BLYP functional^{53,54} (except for the Rb^+ , for which the PBE functional⁵⁵ was used). The Troullier-Martins⁵⁶ (Cl^- , Cs^+ and K^+) and Goedecker-Teter-Hutter^{57–59} (Na^+ , Rb^+ , Mg^{2+} , Ca^{2+} and Sr^{2+}) pseudopotentials were used, with a plane-wave basis set and an energy cutoff of at least 70 Ry. Similarly, configurations of crystals containing between 16 and 108 MCl or MCl_2 units, are used to perform the DFT calculations, with the same functionals and

pseudopotentials as for the ions in water. In each case, after determining the electronic density, the forces acting on each atom are computed and the dipoles are calculated from the MLWFs as described above. The C_6 and C_8 dispersion parameters are computed from the spreads and distances to the center of the MLWFs, which result from the localization procedure. The polarizabilities are calculated as explained above, by applying an external field using the Berry phase representation⁴². All *ab-initio* calculations were performed using the CPMD simulation package⁶⁰ (except for those involving Ca^{2+} , performed with CP2K simulation package⁶¹), while classical forces and dipoles are computed on the same configurations with FIST, the classical MD module of the CP2K simulation package⁶¹. The numerical minimization of Eqs. (16) and (17) is performed using the Minuit library⁶².

F. Parametrization: Results

The computed polarizabilities for all the ions are summarized in table II. As expected, the polarizability increases when going down along columns of the periodic table (alkaline and alkaline earths series), while a decrease is observed when going from left to right along rows (Na^+ to Mg^{2+} , K^+ to Ca^{2+} and Rb^+ to Sr^{2+}). For cations, the condensed phase polarizability is comparable to that in the gas phase, except for Cs^+ . For the chloride anion, however, the confinement of electrons by the surrounding water molecules results in a significant decrease of the polarizability (approximately 35%). A more detailed discussion has been given in Ref.⁴².

Interestingly, as indicated in Table II, the (induced) dipole moment of cations is always very small compared to that of the chloride anion and water. This can be explained by the combination of two factors. First, most cations have a small (K^+ , Sr^{2+}) or very small (Li^+ , Na^+ , Mg^{2+} , Ca^{2+}) polarizability. Second, all cations have a highly symmetric hydration sphere, which results in very weak local electric fields to polarize them. Because the induced dipoles are very small, they are not easily reproduced by the classical force field (typical errors are of the order of 100%), but they do not contribute significantly to the polarization energy V_{pol} , which is dominated by the interaction of the ionic charge with the dipole of water, and hence to the forces. For the sake of simplicity, we thus decided to neglect the polarizability of all cations and not include any additional degrees of freedom to describe their induced dipoles.

Ion	α (\AA^3)	$\sqrt{\langle \mu^2 \rangle}$ (Debye)
Li^+	0.03	0.002
Na^+	0.18	0.014
K^+	0.81	0.062
Rb^+	1.32	0.097
Cs^+	2.02	0.153
Mg^{2+}	0.08	0.010
Ca^{2+}	0.44	0.026
Sr^{2+}	0.81	0.071
Cl^-	3.50	0.415

TABLE II: Polarizability α and magnitude of the induced dipole of each ion $\sqrt{\langle \mu^2 \rangle}$. The latter is 1.18 D for water.

The parameters for the cation-water interaction are summarized in Table III, and those for the chloride-water interaction are given in Table IV. Finally, all parameters for the ion-ion interactions are given in Table V. The resulting repulsion potentials V_{rep} between water and the various cations, plotted in Fig. 2, nicely reflect the expected increase in ionic size along the alkaline and alkaline earth series. Furthermore, a comparable repulsion is observed for isoelectronic species such as Na^+ and Mg^{2+} , K^+ and Ca^{2+} , and Rb^+ and Sr^{2+} . In line with the polarizabilities, the C_6 and C_8 dispersion coefficients for the ion-water interaction increase along the alkaline and alkaline earths series, while a decrease is observed from left to right along rows of the periodic table. The same trends hold for the repulsion and dispersion interactions between the cations and the chloride anion.

We now examine the performance of the force field in terms of reproducing the *ab-initio* dipoles and forces. Figure 3 illustrates the comparison between the forces on the ion calculated with the classical force field (without dispersion) and those obtained from the DFT calculations, for the Ca^{2+} cation. From table VI, the relative error of the force, $\sqrt{\chi_F^2}$, on the Ca^{2+} ion, with respect to the DFT result, is approximately 23% . This can be considered as a good match, especially when comparing to the corresponding results obtained by using the Dang potential⁶³ (with the same water model), which results in a

System	$A^{\text{ion-O}}$ (Ha)	$B^{\text{ion-O}}$ (\AA^{-1})	$C_6^{\text{ion-O}}$ (Ha. \AA^6)	$C_8^{\text{ion-O}}$ (Ha. \AA^8)	b_D^{IJ} (\AA^{-1})	$b^{\text{ion-M}}$ (\AA^{-1})	$c^{\text{ion-M}}$
Li ⁺ -water	24.75	4.094	1.103×10^{-2}	1.037×10^{-2}	3.000	4.011	2.950
Na ⁺ -water	711.1	5.061	1.335×10^{-1}	1.572×10^{-1}	3.000	1.562	6.839×10^{-1}
K ⁺ -water	125.7	3.735	7.530×10^{-1}	1.206	3.000	1.315	4.623×10^{-1}
Rb ⁺ -water	157.8	3.656	1.225	2.267	3.000	1.248	4.765×10^{-1}
Cs ⁺ -water	269.4	3.635	2.040	4.644	1.800	2.524	2.948
Mg ²⁺ -water	65.67	3.963	6.408×10^{-2}	7.23×10^{-3}	-	3.963	2.820
Ca ²⁺ -water	57.94	3.327	5.055×10^{-1}	7.502×10^{-1}	-	3.327	3.000
Sr ²⁺ -water	41.55	2.991	9.159×10^{-1}	1.576	-	2.991	2.041

TABLE III: Parameters for the cation-water interactions. As for water-water interactions, repulsion and dispersion involve the oxygen atom, while electrostatic interactions involve the additional M site. The damping parameter b_D for the dispersion interaction for the monovalent ions is chosen equal to that of the corresponding cation-chloride interaction (see text and table V). The electrostatic damping is between the water dipole and cation charge.

System	$A^{\text{ion-O}}$ (Ha)	$B^{\text{ion-O}}$ (\AA^{-1})	$C_6^{\text{ion-O}}$ (Ha. \AA^6)	$C_8^{\text{ion-O}}$ (Ha. \AA^8)	$b^{\text{ion-H}}$ (\AA^{-1})	$c^{\text{ion-H}}$	$b^{\text{ion-M}}$ (\AA^{-1})	$c^{\text{ion-M}}$
Cl-water	499.63	3.560	2.039	4.296	4.794	1.093	2.444	-1.901

TABLE IV: Parameters for the chloride-water interactions. The dipole damping is between the Cl⁻ and the water charges. For the reasons already explained, there is no damping of the dispersion.

relative error of approximately 320%. Similarly, our results for Sr²⁺ show a relative error of 36%, compared to 501% with the force field from the literature⁶⁴, 49% vs. 66% for Na⁺, 48% vs. 131% for Cs⁺ and 53% vs. 104% for Cl⁻. Overall, the forces on all ions are well reproduced by the present force field. The largest contributions to the relative error (see Eq. 17) correspond to the smaller forces.

Table VII reports the χ^2 values obtained on the crystals for the forces on both cations and anions, as well as for the dipole of the anions. Comparison with Table VI indicates that a similar accuracy is obtained for both the crystals and the ions in solution, suggesting that the force field should perform well under both conditions. This result is also encouraging from the point of view of the transferability and the possible prediction of the solubility of

System	Ion pair IJ	A^{IJ} (Ha)	B^{IJ} (\AA^{-1})	C_6^{IJ} (Ha. \AA^6)	C_8^{IJ} (Ha. \AA^8)	b_D^{IJ} (\AA^{-1})	b^{IJ} (\AA^{-1})	c^{IJ}
LiCl	Li^+-Li^+	481.9	6.958	2.727×10^{-4}	5.570×10^{-10}	6.958	-	-
	Li^+-Cl^-	15.56	3.000	2.369×10^{-2}	2.511×10^{-2}	3.000	3.128	1.433
	$\text{Cl}^- - \text{Cl}^-$	698.4	3.777	5.951	12.85	1.650	-	-
NaCl	Na^+-Na^+	1.701×10^{-2}	4.965	2.914×10^{-2}	1.394×10^{-2}	4.965	-	-
	Na^+-Cl^-	44.43	3.000	2.971×10^{-1}	3.785×10^{-1}	3.000	2.775	2.040
	$\text{Cl}^- - \text{Cl}^-$	698.4	3.777	5.951	12.85	1.650	-	-
KCl	K^+-K^+	174.9	5.000	7.172×10^{-1}	9.260×10^{-1}	5.000	-	-
	K^+-Cl^-	82.92	3.000	1.973	3.347	3.000	1.282	9.059×10^{-1}
	$\text{Cl}^- - \text{Cl}^-$	698.4	3.777	5.951	12.85	1.650	-	-
RbCl	Rb^+-Rb^+	1.235×10^{-2}	3.485	2.235	3.908	3.485	-	-
	Rb^+-Cl^-	108.0	3.000	3.755	7.223	3.000	1.460	9.825×10^{-1}
	$\text{Cl}^- - \text{Cl}^-$	698.4	3.777	5.951	12.85	1.650	-	-
CsCl	Cs^+-Cs^+	353.0	3.782	7.325	18.64	3.782	-	-
	Cs^+-Cl^-	150.1	3.000	7.339	16.96	1.800	1.541	4.665×10^{-1}
	$\text{Cl}^- - \text{Cl}^-$	698.4	3.777	5.951	12.85	1.650	-	-
MgCl ₂	$\text{Mg}^+-\text{Mg}^{2+}$	2.231×10^{-1}	4.995	1.095×10^{-2}	4.066×10^{-3}	4.995	-	-
	$\text{Mg}^{2+}-\text{Cl}^-$	85.84	3.400	1.471×10^{-1}	2.102×10^{-1}	3.400	2.886	2.113
	$\text{Cl}^- - \text{Cl}^-$	698.4	3.777	5.951	12.85	1.650	-	-
CaCl ₂	$\text{Ca}^{2+}-\text{Ca}^{2+}$	1.289×10^{-1}	3.941	3.274×10^{-1}	3.456×10^{-1}	3.941	-	-
	$\text{Ca}^{2+}-\text{Cl}^-$	236.3	3.400	1.168	1.883	3.400	2.052	1.268
	$\text{Cl}^- - \text{Cl}^-$	698.4	3.777	5.951	12.85	1.650	-	-
SrCl ₂	$\text{Sr}^{2+}-\text{Sr}^{2+}$	5.513	4.735	1.259	1.867	4.735	-	-
	$\text{Sr}^{2+}-\text{Cl}^-$	269.4	3.400	2.697	5.066	2.400	3.103	2.939
	$\text{Cl}^- - \text{Cl}^-$	698.4	3.777	5.951	12.85	1.650	-	-

TABLE V: Parameters for the ion-ion interactions.

these crystals. Comparison between tables VII and VIII illustrates the better performance of the present model compared to those of Dang and coworkers^{49–51}.

Neglecting the polarizability of cations does not prevent us from obtaining a good de-

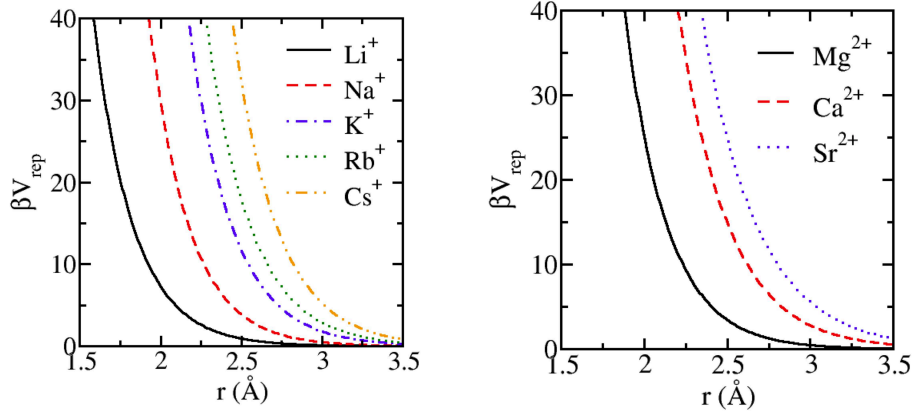


FIG. 2: Repulsion potential between water and alkaline cations (a) and alkaline earth cations (b), in units of the thermal energy $\beta^{-1} = k_B T$.

scription of the forces acting on them, as can be seen in table VI. These forces are even better described than those on the chloride ion, whose polarizability is explicitly taken into account. Nevertheless, for the reasons mentioned in the introduction, it is essential to correctly reproduce the polarization of water molecules around ions. Table VI also indicates the relative error on the dipole of water molecules in the first solvation shell of the ions. The combination of the Dang-Chang water model with the present model for the ion-water interactions provides a very good description of the polarization of water, with relative errors between 5 and 10% for all ions except Mg^{2+} (13%).

III. VALIDATION

Having shown that our force field is able to correctly reproduce the *ab-initio* dipoles and forces, we now turn to its validation against experimental data pertaining to the structure, thermodynamics and dynamics of aqueous ions at infinite dilution, as well as to the density of ionic crystals. We finally investigate the transferability of the force field to concentrated solutions, which were not taken into account when “designing” the force field. It is worth

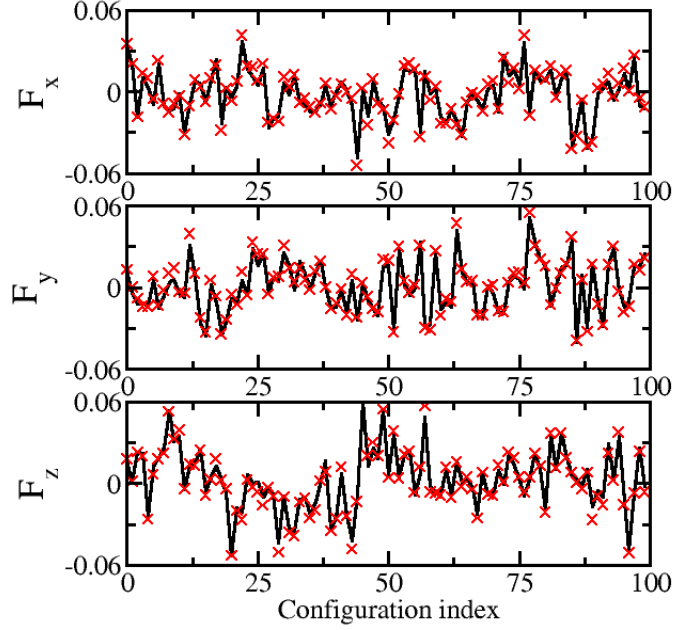


FIG. 3: Force (in atomic units) acting on the Ca^{2+} ion. The prediction of the classical force field (lines) for the 3 components F_x , F_y and F_z are compared to the DFT result (\times), for 100 configurations composed of 32 water molecules and 1 Ca^{2+} .

pointing out here that we use experimental data only for validation purposes, in contrast with all other force fields for aqueous ions, which use some experimental data for calibration of the parameters. Out of the 241 parameters defining the force field for the present set of ions, only 3 (the dispersion damping parameters $b_D^{\text{Cl-Cl}}$, $b_D^{\text{Cs-Cl}}$ and $b_D^{\text{Sr-Cl}}$) are determined with the use of experimental data, namely the densities of the 8 crystals. In particular, no experimental data on aqueous ions is used during the calibration process.

A. Simulation details

For ions at infinite dilution, the system contains a single ion and 215 water molecules in a cubic box of size $L = 18.65 \text{ \AA}$. For the crystals, the systems consist of 256 LiCl, NaCl, KCl or RbCl, 342 CsCl, 192 MgCl_2 or CaCl_2 , or 256 SrCl_2 . Systems for concentrated solutions are composed of 27 NaCl, KCl and 458 water molecules in cubic box of sizes 24.4167 \AA and 24.638 \AA , respectively. Electrostatic interactions are computed using a dipolar Ewald sum^{65,66}, with a tolerance of 1.10^{-7} to obtain the self-consistent dipole moments. Molecular

Ion	$\chi_{\text{F-ion}}^2$	$\chi_{\mu-H_2O}^2$	$\chi_{\mu\text{-ion}}^2$
Li ⁺	1.56×10^{-1}	1.76×10^{-3}	-
Na ⁺	2.36×10^{-1}	7.81×10^{-3}	-
K ⁺	1.11×10^{-1}	2.79×10^{-3}	-
Rb ⁺	1.02×10^{-1}	2.35×10^{-3}	-
Cs ⁺	2.28×10^{-1}	3.08×10^{-3}	-
Mg ²⁺	9.97×10^{-2}	1.78×10^{-2}	-
Ca ²⁺	5.35×10^{-2}	9.05×10^{-3}	-
Sr ²⁺	1.27×10^{-1}	2.73×10^{-3}	-
Cl ⁻	2.84×10^{-1}	3.40×10^{-3}	2.05×10^{-1}

TABLE VI: χ^2 for the forces on the ions and the dipoles of water and the ions.

Crystal	$\chi_{\text{F-M}^{x+}}^2$	$\chi_{\text{F-Cl}^-}^2$	$\chi_{\mu\text{-Cl}^-}^2$
LiCl	1.13×10^{-1}	1.74×10^{-2}	1.91×10^{-1}
NaCl	2.52×10^{-2}	1.12×10^{-2}	1.87×10^{-1}
KCl	7.88×10^{-2}	5.61×10^{-2}	7.28×10^{-1}
RbCl	4.77×10^{-2}	6.46×10^{-2}	6.66×10^{-1}
CsCl	2.23×10^{-2}	1.15×10^{-1}	4.30×10^{-1}
MgCl ₂	2.62×10^{-1}	8.45×10^{-2}	1.90×10^{-2}
CaCl ₂	5.58×10^{-2}	8.46×10^{-3}	2.27×10^{-1}
SrCl ₂	3.61×10^{-2}	3.95×10^{-2}	5.69×10^{-2}

TABLE VII: χ^2 in crystals, for the forces on the cations and anions, and the dipoles of anions.

dynamics in the canonical ensemble are performed using a Nose-Hoover thermostat with a time constant of 1 ps. The system is first equilibrated for 250 ps, and the properties are determined from subsequent 2.75 ns runs. The density of the crystals is determined from simulations in the NPT ensemble at $P = 1$ bar. The thermostat is the same than the one used for the NVT ensemble and the barostat is an extension of the one by Martyna *et al.*⁶⁷. All simulations are performed using the CP2K simulation package⁶¹.

Crystal	$\chi_{\text{F-M}^{x+}}^2$	$\chi_{\text{F-Cl}^{-}}^2$
LiCl	3.51	28.0
NaCl	4.46×10^{-1}	3.50
KCl	4.38	4.10
CsCl	2.24	2.56
CaCl ₂	1.03	9.85×10^{-1}
SrCl ₂	5.47	8.28

TABLE VIII: χ^2 in crystals, for the forces on the cations and anions, with the polarizable Dang-Chang models.

B. Solvation of ions: structure

We first investigate the structure of the solvation shells around ions by computing radial distribution functions, reported for the cations in Fig. 4. As usually observed, the position of the first maximum gradually shifts towards larger distances when switching from Li^+ to Cs^+ and from Mg^{2+} to Sr^{2+} , while the value of the maximum decreases and the peak broadens. On the contrary, moving right along the rows of the periodic table results in a closer and sharper peak. This arises from the stronger electrostatic interaction, since the ion-water repulsion remains comparable, as discussed previously, and reflects a tighter first solvation shell.

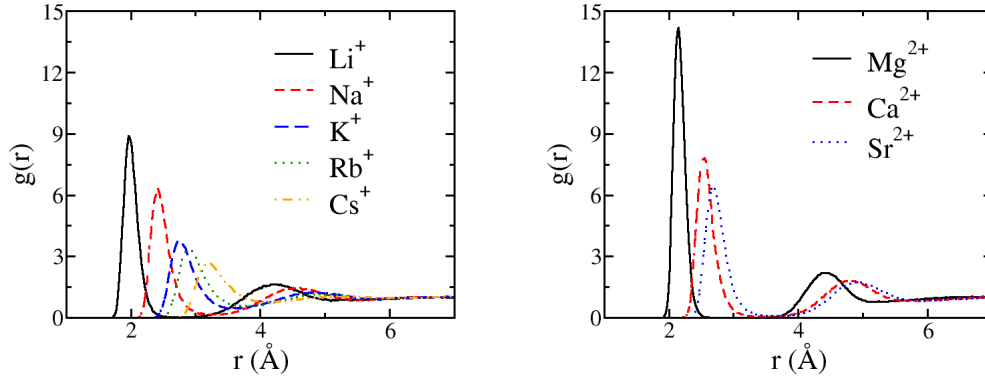


FIG. 4: Ion-oxygen radial distribution functions for the aqueous cations.

The positions of the first maximum and the coordination numbers, defined as the integral of the ion-O(water) radial distribution function from the origin out to the first minimum, are summarized in Table IX, together with the corresponding experimental values. The value and error estimates of the coordination numbers are determined from the plateau of the running values. Remarkably, all simulated data fall in the reported experimental ranges. Particularly encouraging is the agreement with experimental data for the three divalent ions. While several force fields are able to correctly predict the position and number of neighbours for the Mg^{2+} ion, many of them fail to correctly reproduce that of Ca^{2+} . As an example, a force field by Yu *et al.* based on a Drude model of polarizability, which accurately describes the hydration free energies, predicts a coordination number of 6 for this ion⁵². Our result is very close to the value of 7.3 obtained with the popular AMOEBA force field used for biomolecular simulations⁶⁸. The previously available model for Ca^{2+} , with the present water model, predicts a distance of 2.45 Å, within the experimental range, but it used the EXAFS data of 2.43 Å in the parametrization process. In the case of Sr^{2+} , we find a distance very close to the anomalous X-ray diffraction value of 2.67 Å⁶⁹ and a coordination number which is within the reported experimental range.

When comparing simulation results for an ion at infinite dilution with experiments, one should pay attention to the experimental conditions, in particular the concentration and the nature of the counterion. For example, Smirnov and Trostin reported an increase of the Cs^+ coordination number with decreasing concentration⁷⁰. It is thus not surprising to find our result on the larger side of the experimental range. Moreover, results using ClO_4^- as a counterion instead of Cl^- are less likely to be polluted by the formation of ion pairs. The distances of 2.12 and 2.65 Å between the cation and the nearest water oxygen, reported with ClO_4^- in Ref.⁷¹ for Mg^{2+} and Sr^{2+} , respectively, are in very good agreement with ours (2.13 and 2.68).

Since most force fields include some experimental data on the structure during the calibration process^{52,63,64}, it is possible to obtain a good agreement. When such data is not included as a target property, the predicted structure may not be very accurate. As an example, Horinek *et al.* parametrized a simple non-polarizable force field optimized for the simulation of solvation thermodynamics⁷². The structural properties, used only for validation purposes, revealed a tendency to underestimate the distances to the nearest water molecules for cations. Our results for the chloride ion are very good, as they fall exactly on

the EXAFS value of 2.11 Å determined by Dang *et al.*, whereas many force fields tend to predict too large a distance for the first peak^{63,72}, even though they include such structural properties in the fitting procedure⁶³.

Ion	Position (Å)		Coordination Number	
	Sim	Exp	Sim	Exp
Li ⁺	1.96	1.90-2.25	4.0	4
Na ⁺	2.41	2.41-2.50	5.7±0.1	4-8
K ⁺	2.74	2.60-2.92	6.45±0.25	4-8
Rb ⁺	2.88	2.80-3.05	7.05±0.25	6-8
Cs ⁺	3.20	2.95-3.21	8.3±0.8	6-8
Mg ²⁺	2.13	2.00-2.15	6.0	6
Ca ²⁺	2.53	2.40-2.58	7.24±0.02	7-9
Sr ²⁺	2.68	2.57-2.67	7.81±0.05	7.3-10.3
Cl ⁻	3.11	3.05-3.18	6.12±0.12	5.3-6.4

TABLE IX: Structural properties: position of the first maximum in radial distribution function and coordination number. The experimental values are taken from Refs.^{63,69–71,73}

Positions and coordination numbers cannot be measured directly, and the experimental values are the outcome of a complex numerical analysis of the raw data, which typically involves several Fourier transforms and filters which can influence the final result. A more stringent test of the force field thus consists in comparing the experimental signal to that obtained by computing the experimental observables on configurations generated by molecular simulation. An example of such a test is given in Fig. 5, which compares the experimental EXAFS signal for aqueous Ca²⁺, obtained from Ref.⁶³, to that predicted from our configurations using the FEFF8 code, which uses an updated version of the Rehr *et al.* algorithm⁷⁴ to evaluate multiple electron scattering series. The agreement is seen to be very good in the $k > 3 \text{ Å}^{-1}$ part of the spectrum, both in terms of the amplitude (which reflect the number of neighbours) and the frequency of oscillations (related to their position).

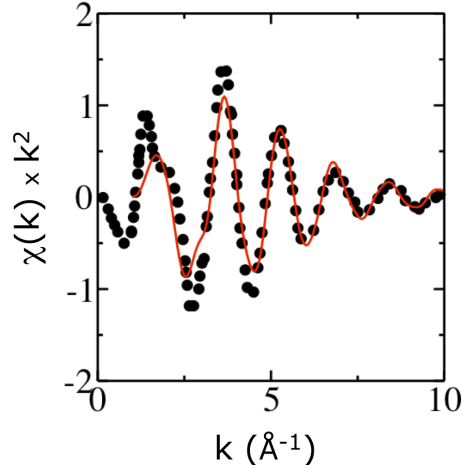


FIG. 5: Comparison between simulated and experimental EXAFS⁶³ signal for aqueous Ca^{2+} . The agreement is very good both for the amplitude, which reflects the number of neighbours, and frequency of the oscillations, related to their position.

C. Solvation of ions: hydration free energy

Among all the ionic properties one aims to predict, the hydration free energy ΔG_{hyd} is probably the most important, since it relates to the ability of ions to accomodate their solvation shell when approaching an interface or other ions. This quantity is almost always one of the target properties used to design force fields. Whereas absolute values are difficult to determine, differences in hydration free energies can be easily computed using a thermodynamic integration procedure without worrying about the numerous corrections^{75,76} (for system size, boundary conditions, and the treatment of electrostatic interactions) needed for the former. The difference $\Delta\Delta G_{\text{hyd}} \approx \Delta\Delta F_{\text{hyd}} = \Delta F_{\text{hyd}}^{\text{K}} - \Delta F_{\text{hyd}}^{\text{Na}}$ can be determined from a thermodynamic path (transmutation) connecting the systems, by introducing a mixed Hamiltonian $H(\lambda) = \lambda H_{\text{K}} + (1 - \lambda)H_{\text{Na}}$ for $\lambda \in [0, 1]$, as

$$\Delta\Delta F = \int_0^1 \left\langle \frac{\partial H}{\partial \lambda} \right\rangle d\lambda \quad (18)$$

For the monovalent ions, we use a 6-point Gaussian quadrature^{77,78} to compute the integral, except for the Li^+ - Cs^+ transmutation, for which we use an 8-point quadrature. Details on this standard quadrature procedure can be found in Ref.⁷⁷. In the case of the divalent ions, where $\partial_\lambda H(\lambda)$ shows a linear variation in λ , a simpler trapezoidal rule can be used to

approximate the integral. In this case we used ten equally spaced points (0.1) for λ_i within the interval $[0, 1]$.

Transmutation	$\Delta\Delta G_{\text{hyd}}^{\text{sim}}$ (kcal/mol)	$\Delta\Delta G_{\text{hyd}}^{\text{exp}}$ (kcal/mol)
$\text{Li}^+ \rightarrow \text{Na}^+$	26.5	[23.8;26.2]
$\text{Na}^+ \rightarrow \text{K}^+$	13.7	[16.7;17.7]
$\text{K}^+ \rightarrow \text{Rb}^+$	3.2	[4.9;5.4]
$\text{Rb}^+ \rightarrow \text{Cs}^+$	7.6	[5.5;7.7]
$\text{Li}^+ \rightarrow \text{Cs}^+$	51.4	[50.9;57.0]
$\text{Mg}^{2+} \rightarrow \text{Ca}^{2+}$	82.2	[77.7;80.3]
$\text{Ca}^{2+} \rightarrow \text{Sr}^{2+}$	25.3	[29.8;32.9]
$\text{Mg}^{2+} \rightarrow \text{Sr}^{2+}$	107.8	[107.5;113.2]

TABLE X: Differences in Gibbs free energy of hydration: Simulated and experimental values. The experimental values for the monovalent ions are taken from references^{79–84} and those for divalent ions from^{81,83,84}.

The hydration free energy differences, for all the transmutations considered, are summarized in Tab. X, together with the corresponding experimental values. The overall agreement with experiment is very good, with deviations never exceeding a few kcal/mol, and the large variations of $\Delta\Delta G_{\text{hyd}}$ across the ion series being well reproduced. We note that some force fields are able to reproduce this quantity slightly more accurately, such as the non-polarizable one of Horinek *et al.*⁸⁵ or the polarizable model (Drude oscillators) of Yu *et al.*⁵². In these cases, however, experimental hydration free energies (or differences) were used as a target property to calibrate the force field, whereas we use it here as an independent validation of our *ab-initio* derived model.

D. Diffusion coefficient

The diffusion coefficient are computed using from the mean-squared displacement, as determined by the Einstein relation :

$$D_{\text{PBC}} = \lim_{t \rightarrow \infty} \frac{1}{6} \frac{\text{d} \langle |\mathbf{r}(t) - \mathbf{r}(0)|^2 \rangle}{\text{d}t} \quad (19)$$

The “PBC” subscript emphasizes the fact that the use of periodic boundary conditions induces a box length dependence on the measured diffusion coefficient, which takes the form⁸⁶:

$$D_{\text{PBC}} = D_0 - \frac{2.837k_B T}{6\pi\eta L} \quad (20)$$

where η is the shear viscosity of the solvent. For the box length of $L = 18.65 \text{ \AA}$ used in our simulations, the correction to the Dang-Chang water model is approximately $0.43 \text{ } 10^{-9} \text{ m}^2\text{s}^{-1}$ and must not be neglected ($D_0^{\text{H}_2\text{O}} = 2.72 \pm 0.09 \text{ m}^2\text{s}^{-1}$)⁸⁷. For a meaningful comparison with experiments, we thus extrapolate to the infinite box length limit, both for the ion and the water diffusion coefficients and compare the ratios $D_0^{\text{ion}}/D_0^{\text{H}_2\text{O}}$.

Ion	$(D_0^{\text{ion}}/D_0^{\text{H}_2\text{O}})_{\text{sim}}$	$(D^{\text{ion}}/D^{\text{H}_2\text{O}})_{\text{exp}}$
Li ⁺	0.49	0.44
Na ⁺	0.54	0.58
K ⁺	0.78	0.88
Rb ⁺	0.88	0.90
Cs ⁺	0.82	0.89
Mg ²⁺	0.31	0.31
Ca ²⁺	0.35	0.34
Sr ²⁺	0.35	0.34
Cl ⁻	0.71	0.88

TABLE XI: Ratio between the ion and water diffusion coefficients. The experimental values for the ions are taken from⁸⁸, the one for the water from⁸⁹.

The simulation results are compared to the experimental ratios in Tab. XI. The relative error is of only 2 to 11% for the monovalent cations. The agreement is particularly good for the divalent cations, for which the relative error does not exceed 3%. The largest relative error is for the Cl⁻ ion (19%). We performed similar simulations with the force field of Dang and co-workers^{49–51}, which uses the same water model. The errors in that case reach 31% for Cl⁻ and 9% for Ca²⁺ and Sr²⁺. Moreover, while our results capture the equal diffusion coefficients of these two cations, the model of Dang and co-workers underestimates that of Ca²⁺ and overestimates that of Sr²⁺.

Since force fields generally do not include experimental data on the dynamics for their calibration, their accuracy for dynamical properties is usually not as high as for structural and thermodynamic ones. The present strategy, which aims at reproducing the forces on the atoms and molecules, as best as possible, allows us to also predict the dynamic properties.

E. Crystal density

As a test of the interactions between ions, we now turn to the study of the ionic crystals. As explained above, out of the 241 parameters defining the force field for the entire family of ions we have studied, only 3 (the dispersion damping parameters $b_D^{\text{Cl-Cl}}$, $b_D^{\text{Cs-Cl}}$ and $b_D^{\text{Sr-Cl}}$) were determined using the experimental densities of the 8 crystals as target properties. All the systems we studied preserved their correct crystal structure during the entire length of the simulations, even the more complex ones corresponding to the divalent cations. Fig. 6 illustrates the deformed rutile structure of CaCl_2 and the lamellar one of MgCl_2 . While a complete study of the relative stability of the different possible phases exceeds the scope of the present work, this suggests that these phases are at least metastable. The simulated densities are compared to the experimental ones in Tab. XII. The overall agreement is once again good, with relative errors below 10% except for NaCl (16%).

Crystal	$\rho_{\text{sim}} \text{ (g.cm}^{-3}\text{)}$	$\rho_{\text{exp}} \text{ (g.cm}^{-3}\text{)}$
LiCl	2.01	2.07
NaCl	1.83	2.17
KCl	1.93	1.99
RbCl	2.98	2.76
CsCl	4.42	3.99
MgCl_2	2.21	2.33
CaCl_2	2.04	2.15
SrCl_2	3.25	3.05

TABLE XII: Density of the crystals at 1 bar and 300 K. The experimental values are taken from⁸⁸. Note that the correct crystal structures (separated in the table) are preserved during the simulations.

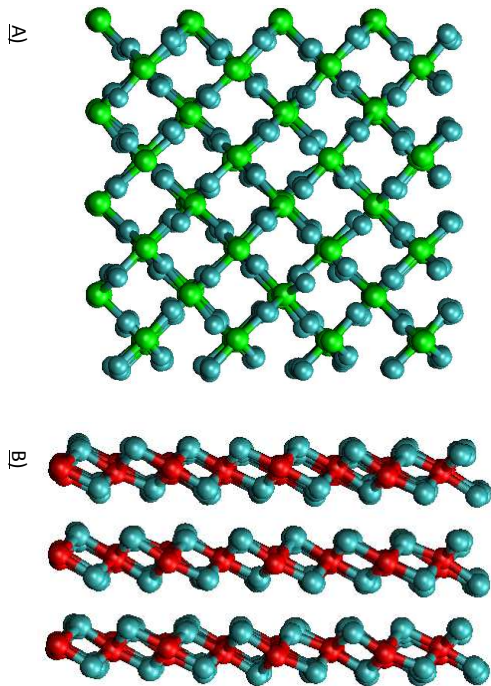


FIG. 6: A) Snapshot of CaCl_2 cristal. B) Snapshot of MgCl_2 cristal. Both structures are stable during the simulations. Cl^- are in cyan, Mg^{2+} in red and Ca^{2+} in green.

Transferability to crystals is rarely tested, making comparisons with other potentials rather difficult. We have again used the force fields of Dang and coworkers^{49–51} to assess the reliability of our potentials. Although their potentials give good results for NaCl ($d=2.1 \text{ g.cm}^{-3}$), KCl (1.9 g.cm^{-3}) and CsCl (3.8 g.cm^{-3}) crystals, the structure proves to be unstable for LiCl , CaCl_2 and SrCl_2 . This example shows the need for more complicated force fields (with more parameters), as they can provide better transferability.

F. Concentrated solutions

The previous sections demonstrate the accuracy of the present force field for both infinitely dilute solutions and crystals. We now test its transferability to conditions which were not considered during the construction of the force field, by investigating concentrated

ionic solutions. We compute the neutron diffraction spectra for concentrated NaCl and KCl solutions with one ion pair for 17 water molecules (1:17) from the site-site partial structure factor between site α and β :

$$S_{\alpha\beta}(Q) = 4\pi\rho \int r^2(g_{\alpha\beta}(r) - 1) \frac{\sin(Qr)}{Qr} dr \quad (21)$$

where ρ is the atomic number density of the solution and $g_{\alpha\beta}(r)$ the corresponding site-site radial distribution function. Experimental neutron diffraction allows for the extraction of composite partial structure factors. We compare our simulations results to the traditionally used F_{XX} function, defined as:

$$F_{XX}(Q) = \frac{\sum_{\alpha,\beta} (2 - \delta_{\alpha\beta}) c_{\alpha} c_{\beta} b_{\alpha} b_{\beta} S_{\alpha\beta}(Q)}{(\sum_{\alpha} c_{\alpha} b_{\alpha})^2} \quad (22)$$

where the sums over α and β run over all atom types except hydrogen and c_{α} and b_{α} are the atomic fraction and neutron scattering length of atom α , respectively. The comparison with the experimental results taken from Ref.⁹⁰ in Figs. 7 and 8 indicates a very good agreement, which confirms the transferability to concentrated solutions.

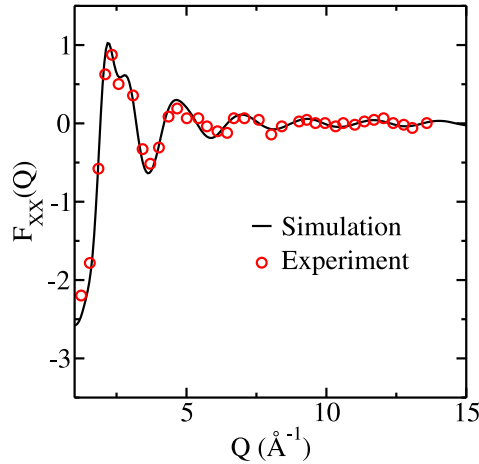


FIG. 7: Comparison between simulated and experimental $F_{XX}(Q)$ from Ref.⁹⁰ for a concentrated NaCl solution (one NaCl pair for 17 water molecules).

IV. CONCLUSION

We have shown a successful parametrization of a polarizable force field for aqueous solutions of Li^+ , Na^+ , K^+ , Rb^+ , Cs^+ , Mg^{2+} , Ca^{2+} , Sr^{2+} and Cl^- ions. We used the polarizable

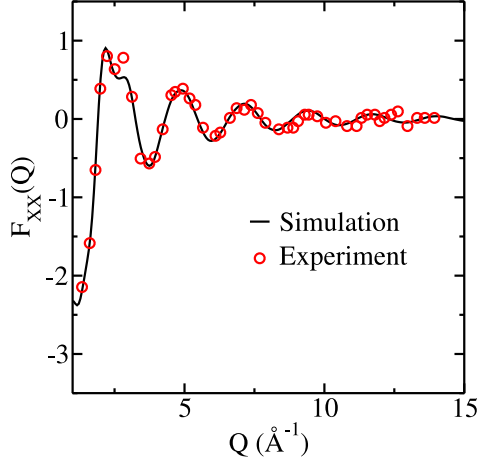


FIG. 8: Comparison between simulated and experimental $F_{XX}(Q)$ from Ref.⁹⁰ for a concentrated KCl solution (one NaCl pair for 17 water molecules).

Dang-Chang model for water and derived all the parameters involving ions in the framework of the polarizable ion model of Madden and co-workers. The procedure relies only on *ab-initio* DFT calculations; part of the parameters (polarizabilities, dispersion coefficients) are directly calculated while the others are extracted from a generalized force- and dipole-matching procedure. Experimental information is used for validation purposes only: The structural (first-neighbour distances, coordination numbers), thermodynamic (hydration free energy differences) and dynamic (diffusion coefficients) are very well reproduced. The interactions between cations and the chloride anion are parametrized on calculations performed in the crystal phases, thus ensuring the accuracy of the force field across the whole concentration range.

The account of multi-body effects via the polarizability should ensure a good transferability to more complex conditions: mixtures of these salts, high temperature and pressure⁹¹ and to liquid-vapor or liquid-solid interfaces. The next step will consist in extending the present approach to the interaction of water with the surface of oxide materials. It will then be possible to use this force field for the study of important problems of environmental science such as the retention of radionuclides onto clay minerals, or the water uptake by clays and zeolites.

Acknowledgments

The authors acknowledge financial support from the Agence Nationale de la Recherche under grant ANR-09-SYSC-012 and from the Groupement National de Recherches PARIS. We also would like to thank Pr. Fabio Bruni and Pr. Alan K. Soper for providing us with the raw data of Ref.⁹⁰.

-
- ¹ J. Heyda, J. C. Vincent, D. J. Tobias, J. Dzubiella, and P. Jungwirth, *J. Phys. Chem. B* **114**, 1213 (2010).
 - ² H. I. Ingolfsson, Y. H. Li, V. V. Vostrikov, H. Gu, J. F. Hinton, R. E. Koeppe, and B. Roux, *J. Phys. Chem.* **115**, 7417 (2011).
 - ³ C. Domene, S. Vemparala, S. Furini, K. Sharp, and M. L. Klein, *J. Am. Chem. Soc.* **130**, 3389 (2008).
 - ⁴ P. Jungwirth and D. Tobias, *Chem. Rev.* **106**, 1259 (2006).
 - ⁵ B. Rotenberg, J.-P. Morel, V. Marry, P. Turq, and N. Morel-Desrosiers, *Geochim. Cosmochim. Acta* **73**, 4034 (2009).
 - ⁶ J.-P. Piquemal, L. Perera, G. A. Cisneros, P. Ren, L. G. Pedersen, and T. A. Darden, *J. Chem. Phys.* **125**, 054511 (2006).
 - ⁷ G. A. Tribello, F. Bruneval, C. Liew, and M. Parrinello, *J. Phys. Chem. B* **113**, 11680 (2009).
 - ⁸ T.-M. Chang and L. X. Dang, *Chem. Rev.* **106**, 1305 (2006).
 - ⁹ C. D. Wick, I.-F. W. Kuo, C. J. Mundy, and L. X. Dang, *J. Chem. Theory Comput.* **3**, 2002 (2007).
 - ¹⁰ A. Aguado, L. Bernasconi, S. Jahn, and P. A. Madden, *Faraday Discuss.* **124**, 171 (2003).
 - ¹¹ D. Marrocchelli, M. Salanne, and P. Madden, *J. Phys.: Condens. Matter* **22**, 152102 (2010).
 - ¹² M. Burbano, D. Marrocchelli, B. Yildiz, H. L. Tuller, S. T. Norberg, S. Hull, P. A. Madden, and G. W. Watson, *J. Phys.: Condens. Matter* **23** (2011).
 - ¹³ S. Jahn and P. Madden, *Phys. Earth Planet. Inter.* **162**, 129 (2007).
 - ¹⁴ D. L. Newell, J. P. Kaszuba, H. S. Viswanathan, R. J. Pawar, and T. Carpenter, *Geophys. Res. Lett.* **35**, L23403 (2008).
 - ¹⁵ R. M. Espinosa-Marzal and G. W. Scherer, *Acc. Chem. Res.* **43**, 897 (2010).

- ¹⁶ M. A. Glaus, B. Baeyens, M. H. Bradbury, A. Jakob, L. R. Van Loon, and A. Yaroshchuk, *Environ. Sci. Technol.* **41**, 478 (2007).
- ¹⁷ T. Gimmi and G. Kosakowski, *Environ. Sci. Technol.* **45**, 1443 (2011).
- ¹⁸ W. Jorgensen, J. Chandrasekhar, J. Madura, R. Impey, and M. Klein, *J. Chem. Phys.* **79**, 926 (1983).
- ¹⁹ H. Berendsen, J. Grigera, and T. Straatsma, *J. Phys. Chem.* **91**, 6269 (1987).
- ²⁰ J. L. F. Abascal and C. Vega, *Phys. Rev. Lett.* **98**, 237801 (2007).
- ²¹ C. Vega and L. F. Abascal, *Phys. Chem. Chem. Phys.* **13**, 19663 (2011).
- ²² P. J. van Maaren and D. van der Spoel, *J. Phys. Chem. B* **105**, 2618 (2001).
- ²³ T. Hansson, H. Yu, and W. F. van Gunsteren, *J. Chem. Phys.* **118**, 221 (2003).
- ²⁴ A. D. MacKerell, G. Lamoureux, and B. Roux, *J. Chem. Phys.* **119**, 5185 (2003).
- ²⁵ M. Sprik, *J. Phys. Chem.* **95**, 2283 (1991).
- ²⁶ S. J. Stuart, S. W. Rick, and B. J. Berne, *J. Chem. Phys.* **101**, 6141 (1994).
- ²⁷ J. Caldwell and P. Kollman, *J. Phys. Chem.* **99**, 6208 (1995).
- ²⁸ B. J. Berne and A. Wallqvist, *J. Phys. Chem. A* **97**, 13941 (1993).
- ²⁹ L. X. Dang and T.-M. Chang, *J. Chem. Phys.* **106**, 8149 (1997).
- ³⁰ A. A. Chialvo and P. T. Cummings, *J. Chem. Phys.* **105**, 8274 (1996).
- ³¹ J. Sala, E. Guardia, and M. Masia, *J. Chem. Phys.* **133**, 234101 (2010).
- ³² M. Masia, M. Probst, and R. Rey, *J. Chem. Phys.* **121**, 7362 (2004).
- ³³ M. Masia, M. Probst, and R. Rey, *J. Chem. Phys.* **123**, 164505 (2005).
- ³⁴ R. Heaton, R. Brookes, P. Madden, M. Salanne, C. Simon, and P. Turq, *J. Phys. Chem. B* **110**, 11454 (2006).
- ³⁵ N. Ohtori, M. Salanne, and P. Madden, *J. Chem. Phys.* **130**, 104507 (2009).
- ³⁶ N. Marzari and D. Vanderbilt, *Phys. Rev. B* **56**, 12847 (1997).
- ³⁷ B. Rotenberg, M. Salanne, C. Simon, and R. Vuilleumier, *Phys. Rev. Lett.* **104**, 138301 (2010).
- ³⁸ P. Madden, R. Heaton, A. Aguado, and S. Jahn, *J. Mol. Struct.: THEOCHEM* **771**, 9 (2006).
- ³⁹ M. Salanne, B. Rotenberg, S. Jahn, R. Vuilleumier, C. Simon, and P. A. Madden, *Theor. Chem. Acc.* **131**, 1143 (2012).
- ⁴⁰ K. Tang and J. Toennies, *J. Chem. Phys.* **80**, 3726 (1984).
- ⁴¹ R. M. Martin, Electronic structure basic theory and practical methods (Cambridge University Press, 2004).

- 42 J. J. Molina, S. Lectez, S. Tazi, M. Salanne, J. F. Dufreche, J. Roques, E. Simoni, P. A. Madden, and P. Turq, *J. Chem. Phys.* **134**, 014511 (2011).
- 43 S. Grimme, *J. Comput. Chem.* **25**, 1463 (2004).
- 44 P. L. Silvestrelli, *Phys. Rev. Lett.* **100**, 053002 (2008).
- 45 Y. Andersson, D. C. Langreth, and B. I. Lundqvist, *Phys. Rev. Lett.* **76**, 102 (1996).
- 46 R. O. Jones and O. Gunnarsson, *Rev. Mod. Phys.* **61**, 689 (1989).
- 47 S. Kristyàn and P. Pulay, *Chem. Phys. Lett.* **229**, 175 (1994).
- 48 A. J. Stone, Theory of intermolecular forces (Oxford University Press, Oxford, 1996).
- 49 L. X. Dang, *J. Chem. Phys.* **96**, 6970 (1992).
- 50 T.-M. Chang and L. X. Dang, *J. Phys. Chem. B* **101**, 10518 (1997).
- 51 L. X. Dang and T.-M. Chang, *J. Phys. Chem. B* **106**, 235 (2002).
- 52 H. Yu, T. W. Whitfield, E. Harder, G. Lamoureux, I. Vorobyov, V. M. Anisimov, J. A. D. MacKerell, and B. Roux, *J. Chem. Theory Comput.* **6**, 774 (2010).
- 53 A. Becke, *Phys. Rev. A* **38**, 3098 (1988).
- 54 C. Lee, W. Yang, and R. Parr, *Phys. Rev. B* **37**, 785 (1988).
- 55 J. Perdew, K. Burke, and M. Ernzerhof, *Phys. Rev. Lett.* **77**, 3865 (1996).
- 56 N. Troullier and J. Martins, *Phys. Rev. B* **43**, 001993 (1991).
- 57 S. Goedecker, M. Teter, and J. Hutter, *Phys. Rev. B* **54**, 1703 (1996).
- 58 C. Hartwigsen, S. Goedecker, and J. Hutter, *Phys. Rev. B* **58**, 1703 (1998).
- 59 M. Krack, *Theor. Chem. Acc.* **114**, 145 (2005).
- 60 The CPMD consortium, CPMD version 3.13.2, URL <http://www.cpmc.org>.
- 61 CP2K developers group, URL <http://cp2k.berlios.de>.
- 62 F. James and M. Roos, *Comp. Phys. Commun.* **10**, 343 (1975).
- 63 L. X. Dang, G. K. Schenter, V.-A. Glezakou, and J. L. Fulton, *J. Chem. Phys. B* **110**, 23644 (2006).
- 64 L. X. Dang, G. K. Schenter, and J. L. Fulton, *J. Phys. Chem. B* **107**, 14119 (2003).
- 65 A. Aguado and P. A. Madden, *J. Chem. Phys.* **119**, 7471 (2003).
- 66 T. Laino and J. Hutter, *J. Chem. Phys.* **129**, 074102 (2008).
- 67 G. Martyna, D. Tobias, and M. Klein, *J. Chem. Phys.* **101**, 4177 (1994).
- 68 D. Jiao, C. King, A. Grossfield, T. A. Darden, and P. Ren, *J. Phys. Chem. B* **110**, 18553 (2006).
- 69 S. Ramos, G. W. Neilson, A. C. Barnes, and M. J. Capitan, *J. Chem. Phys.* **118**, 5542 (2003).

- ⁷⁰ P. R. Smirnov and V. N. Trostin, *Rus. J. Phys. Chem* **77**, 2101 (2007).
- ⁷¹ H. Ohtaki and T. Radnal, *Chem. Rev.* **93**, 1157 (1993).
- ⁷² D. Horinek, S. I. Mamatkulov, and R. R. Netz, *J. Chem. Phys.* **130**, 124507 (2009).
- ⁷³ Y. Marcus, *Chem. Rev.* **109**, 1346 (2009).
- ⁷⁴ J. J. Rehr, R. C. Albers, and S. I. Zabinsky, *Phys. Rev. Lett.* **69** (1992).
- ⁷⁵ M. Kastenholz and P. Hunenberger, *J. Chem. Phys.* **124**, 124106 (2006).
- ⁷⁶ M. A. Kastenholz and P. Hunenberger, *J. Chem. Phys.* **124**, 224501 (2006).
- ⁷⁷ W. Press, B. Flannery, S. Teukolsky, and W. Vetterling, Numerical Recipes: the art of scientific computing (Cambridge University Press, 1992), 2nd ed.
- ⁷⁸ F. B. Hildebrand, Introduction to numerical analysis (Dover publications, 1987).
- ⁷⁹ M. D. Tissandier, K. A. Cowen, W. Y. Feng, E. Gundlach, M. H. Cohen, A. D. Earhart, and J. V. Coe, *J. Phys. Chem. A* **102**, 7787 (1998).
- ⁸⁰ J. E. B. Randles, *Trans. Faraday Soc.* **52**, 1573 (1956).
- ⁸¹ R. Schmid, A. M. Miah, and V. N. Sapunov, *Phys. Chem. Chem. Phys.* **2**, 97 (2000).
- ⁸² R. M. Noyes, *J. Am. Chem. Soc.* **84**, 513 (1962).
- ⁸³ R. Gomer and G. Tryson, *J. Chem. Phys.* **66**, 4413 (1977).
- ⁸⁴ Y. Marcus, *J. Chem. Soc., Faraday Trans.* **87**, 2995 (1991).
- ⁸⁵ D. Horinek, S. I. Mamatkulov, and R. R. Netz, *J. Chem. Phys.* **130** (2009).
- ⁸⁶ I.-C. Yeh and G. Hummer, *J. Phys. Chem. B* **108**, 15873 (2004).
- ⁸⁷ S. Tazi, A. Botan, M. Salanne, V. Marry, P. Turq, and B. Rotenberg, *J. Phys.: Condens. Matter* in press.
- ⁸⁸ D. R. Lide, ed., CRC Handbook of Chemistry and Physics (85th ed) (Taylor and Francis: Boca raton, FL, 2005).
- ⁸⁹ K. Krynicki, C. D. Green, and D. W. Sawyer, *Faraday Discuss.* **66**, 199 (1978).
- ⁹⁰ R. Mancinelli, A. Botti, F. Bruni, M. A. Ricci, and A. K. Soper, *Phys. Chem. Chem. Phys.* **9**, 2959 (2007).
- ⁹¹ S. Klotz, L. E. Bove, T. Strässle, T. C. Hansen, and A. M. Saitta, *Nature Mater.* **8**, 405 (2009).